https://doi.org/10.1590/jatm.v18.1460

ORIGINAL PAPER

Influence of Boron on the Performance of Solid Fuel Ramjet Propulsion: A Reduced-Order Modeling Approach

Jorge Fernando Leite Monteiro Júnior[1,*], Fausto Mendonça[1]

1. Departamento de Ciência e Tecnologia Aeroespacial – Instituto Tecnológico de Aeronáutica – Departamento de Química – São José dos Campos/SP – Brazil.

*Corresponding author: jorgejota81@gmail.com

ABSTRACT

This study investigates the flight performance of a solid-fuel ramjet missile, comparing a conventional hydroxyl-terminated polybutadiene propellant against a formulation enriched with 33% boron. A computational framework was developed in Python, coupling NASA Chemical Equilibrium with Applications-based thermochemical equilibrium data with a high-fidelity flight dynamics model that accounts for atmospheric variability, instantaneous aerodynamic drag, and continuous mass depletion. To ensure a realistic assessment of energetic potential, a semi-empirical boron combustion efficiency model – sensitive to combustion chamber pressure and temperature – was integrated into the simulation. Results indicate that the boron-loaded propellant significantly expands the operational envelope, yielding a 34.3% increase in specific impulse and extending the effective range by approximately 15.2%. Furthermore, sensitivity analysis across varying payload masses (150 kg to 220 kg) demonstrates that boron's superior energy density provides a performance buffer; notably, a 220 kg boron-fueled missile maintains higher cruise Mach numbers than a lighter conventional counterpart. These findings underscore the strategic utility of metallic additives in enhancing the tactical flexibility and range of next-generation supersonic propulsion systems.

Keywords: Boron; Ramjet engine; Combustion efficiency; Computational chemistry; Solid propellants.

INTRODUCTION

The ramjet engine is a simplified variant of the jet engine, operating on the principle of air compression achieved via the "ram effect" through a supersonic air intake. In this process, air flows through an inlet that generates oblique and/or normal shock waves, thereby increasing both the pressure and temperature of the incoming air. Subsonic combustion then occurs within the combustion chamber, and thrust is produced by the expansion of the working fluid through a convergent-divergent nozzle (Mandal *et al.* 2023).

This type of engine relies solely on its forward motion to compress air; it has no moving parts, enabling it to achieve higher Mach numbers, typically ranging from Mach 3 to Mach 6. However, the ramjet requires an auxiliary propulsion system to accelerate it to its supersonic operating speed (Fry 2004; Ou *et al.* 2017). Notable among the various ramjet engine configurations are the liquid fuel ramjet, solid fuel ramjet (SFRJ), and ducted rocket, each with its own distinctive characteristics (Fry 2004). The SFRJ, in particular, stands out for its mechanical simplicity; its most basic configuration consists of an air intake system, an exhaust nozzle, and a combustion chamber with solid fuel molded into its walls, containing no moving parts. Its operation is based on ablation combustion, where the fuel burn rate naturally adjusts to air density based on altitude. However, it requires additional flow control systems to optimize trajectory and efficiency. To maximize performance, metals such as aluminum or boron are

Received: Apr. 19, 2026 | **Accepted:** July 13, 2026
Peer Review History: Single Blind Peer Review.
Section editor: José Rocco

typically added to the fuel, and internal mixers are used to ensure complete combustion. The greatest challenge for designers lies in balancing the aerodynamics of the air intake with the complex chemistry of diffusion-controlled combustion under different flight conditions (Fry 2004; Krishnan and George 1998).

To maximize combustion performance, the solid propellant uses boron as an additive in quantities greater than those used in traditional rocket engines. These boron-based formulations typically contain ammonium perchlorate (AP) (25–28%), boron (10–45%), aluminum/magnesium (6–8%), and carboxyl-terminated polybutadiene/hydroxyl-terminated polybutadiene (HTPB) (20–30%) (Mandal *et al.* 2023).

Aluminum, magnesium, and boron act as reducing agents in solid propellant formulations to increase the specific impulse (I_{sp}) of the device; however, in these fuels, boron is the primary reducing agent. Boron has a high energy density of 58.1 $kJ \cdot g^{-1}$ and the highest volumetric energy density (136.5 $kJ \cdot cm^{-3}$) when compared to other reducing agents such as aluminum, which has an energy density of 30.8 $kJ \cdot g^{-1}$; however, burning boron is difficult to achieve, so in fuel formulations, the presence of magnesium and aluminum helps reduce ignition delay and increase the burn rate of boron (Yang *et al.* 2023). In these formulations, the resin acts as a continuous phase that binds all the solid particles of the reducing agent and oxidizer, while also providing the mechanical properties of the propellant grain; it must be compatible, for example, with thermal shields and metal components.

A distinctive feature of these fuels is that they are fuel-rich solid propellants that utilize oxygen from the air as their primary oxidizer, which significantly increases the range of the equipment that uses them (Pang *et al.* 2019). Boron has a high heat of combustion per unit volume, nearly three times that of common hydrocarbon fuels. Compared to aluminum, the current standard for high-performance propulsion, boron has a volumetric heat of combustion that is approximately 61% higher and a gravimetric heat of combustion that is approximately 86% higher, assuming complete combustion (Liang *et al.* 2015; Sandall *et al.* 2017) However, boron has high melting and boiling points, is difficult to ignite (requires a large amount of oxygen), and its combustion products can agglomerate, resulting in low combustion efficiency in practical applications (Liang *et al.* 2015).

There are, however, challenges associated with the use of boron in solid fuels. During boron combustion, an oxide layer forms on the surface of the boron particles, creating a barrier between the unreacted boron and the oxygen. Consequently, the molten exterior of the particles on the fuel surface increases particle adhesion and agglomeration, further hindering dispersion. Large boron agglomerates, therefore, require long residence times, making it increasingly difficult to completely burn the boron before it exits the gas generator. The presence of an oxide layer results in a two-step combustion process for boron particles, in which the reaction with oxidizing species is diffusion-limited until the oxide layer is removed, exposing the kinetically limited boron. In general, induction times for boron particles are reported to be longer compared to those for aluminum (Sandall *et al.* 2017).

Several strategies have been adopted to enhance the combustion of boron particles in solid fuels. One effective approach is the inclusion of polytetrafluoroethylene (PTFE), whose decomposition gases react directly with boron oxide to strip away the inhibitive surface layer. This rapid removal accelerates the transition to the second phase of combustion. Beyond PTFE, other reported methods to optimize performance include the use of nano-boron, fluorine-containing compounds, and mechanical activation with auxiliary metals. For instance, the addition of magnesium – noted for its relatively low melting point of 923 K – has been shown to significantly improve reaction kinetics (Pang *et al.* 2019; Sandall *et al.* 2017).

Boron combustion efficiency is intrinsically tied to temperature, pressure, and particle size. Sustained combustion typically demands temperatures exceeding 1900 K (Gany 2014). Increasing the operating pressure further bolsters efficiency by reducing ignition delay and total burn time, primarily by accelerating the evaporation of the protective oxide layer. Conversely, the presence of liquid phases can inhibit oxidation, necessitating high thermal energy to maintain or evaporate the coating. Furthermore, amorphous boron with finer particle sizes generally outperforms larger variants due to faster ignition and enhanced reactivity (Liang *et al.* 2017; Liu *et al.* 2026).

Consequently, accurately predicting the performance of boron-loaded fuels requires models that bridge thermochemical equilibrium calculations with physically grounded descriptions of metal combustion. While detailed multiphase models capture intricate particle-scale phenomena, they remain computationally prohibitive for system-level studies. Reduced-order models (ROMs), which leverage semi-empirical correlations, offer a compelling alternative, enabling the evaluation of boron chemistry within broader propulsion and flight simulations.

The present work investigates the thermochemical performance of boron-loaded solid fuels in ramjet propulsion using a reduced-order modeling framework. Thermodynamic properties of the reacting mixtures are evaluated using equilibrium chemistry calculations obtained through the National Aeronautics and Space Administration (NASA) Chemical Equilibrium with Applications (CEA). To account for incomplete metal combustion, a semi-empirical efficiency model is introduced in which the effective combustion efficiency of boron depends on flame temperature and chamber pressure. This approach enables the energetic contribution of boron to be evaluated under realistic ramjet operating conditions while maintaining computational simplicity.

The primary objective of this study is to quantify the energetic advantages and practical combustion limitations associated with boron-containing solid fuels. By comparing baseline hydrocarbon formulations with boron-enriched mixtures, the analysis seeks to identify the conditions under which the addition of boron provides measurable performance benefits. Particular attention is given to the influence of temperature and pressure on boron combustion efficiency and their impact on overall propulsion performance.

Through this analysis, the work aims to contribute to the understanding of how metal-based fuels can be effectively incorporated into air-breathing propulsion systems and to provide a practical modeling approach for evaluating their thermochemical performance in preliminary propulsion studies.

METHODOLOGY

Overview

In SFRJ configurations, a fuel-rich propellant generates high-enthalpy gases that subsequently undergo aerodynamic mixing with secondary compressed air. While the incorporation of metallic additives – specifically aluminum, magnesium, or boron – significantly enhances volumetric energy density, it introduces complex multiphase phenomena and substantial kinetic constraints. Capturing these effects typically necessitates multidimensional reactive simulations, commonly implemented via computational fluid dynamics integrated with detailed chemical kinetics.

Nevertheless, the conceptual design phase requires ROMs to enable rapid parametric analysis, trend identification, and efficient design space exploration. To address this, an integrated one-degree-of-freedom (1-DOF) flight dynamics and propulsion model is presented. Thermochemical performance is characterized using the RocketCEA framework (derived from the NASA CEA code), which computes equilibrium compositions under specified pressure and equivalence ratios.

The proposed framework couples classical propulsion relations and compressible flow theory with aerodynamic drag formulations. Figure 1 delineates the simulation architecture, illustrating the logical flow and the physical causal chain executed within the Python-based iterative solver.

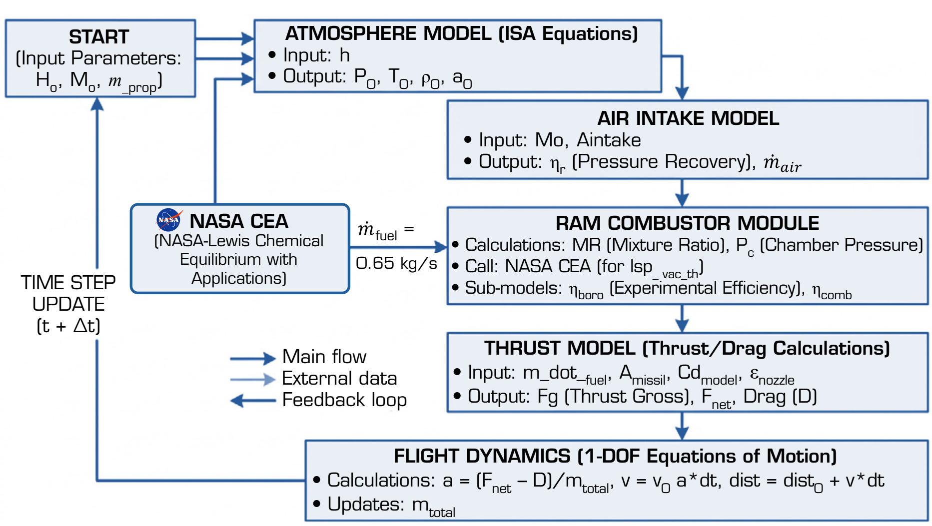

Source: Elaborated by the authors.

Figure 1. Simulation model architecture (SFRJ-1D).

The computational framework presented herein is subject to inherent limitations associated with the NASA CEA code, which operates under the assumption of isentropic, complete thermochemical equilibrium. Consequently, the model predicts the theoretical upper bound of propulsive performance for the reaction mixture (Gordon *et al.* 1984). In practice, however, boron-loaded fuels are characterized by significant combustion inefficiencies stemming from the formation of a persistent, viscous liquid oxide layer (B_2O_3) on the particle surface. This B_2O_3 film acts as a diffusion barrier, impeding the transport of gaseous oxidizers to the reactive boron core and effectively prolonging the ignition delay. These kinetic constraints are particularly pronounced under the moderate temperature and pressure regimes typical of certain ramjet operating conditions (Ao *et al.* 2014; Liang *et al.* 2017; Yeh and Kuo 1996). To mitigate this discrepancy between theoretical equilibrium and experimental reality, a semi-empirical combustion efficiency correlation was integrated to adjust the idealized CEA outputs.

Mathematical formulation and numerical model

The propulsive performance and trajectory of the SFRJ system were characterized using a computational algorithm that couples thermochemical equilibrium manifolds with the kinematic evolution of the flight vehicle. The analysis employs a 1-DOF framework, assuming a standard atmosphere and a quasi-steady-state combustion regime discretized across infinitesimal time steps. The governing equations detailed herein encapsulate the coupled interactions between the supersonic inlet recovery, the enthalpy release within the combustor – modulated by a semi-empirical boron combustion efficiency model – and the resulting aerodynamic and inertial responses.

Propellant formulation

To quantify the thermochemical impact of boron enrichment on SFRJ performance, two distinct propellant formulations were characterized for numerical analysis. The chemical compositions were engineered to maintain a balance between the mechanical integrity of the fuel grain and the maximization of gravimetric I_{sp}.

- Baseline formulation (HTPB/AP): this conventional system comprises 40% HTPB by mass as the binder and 60% AP as the crystalline oxidizer. This composition serves as a benchmark, representing established standards in SFRJ propulsion. For the thermochemical equilibrium calculations in RocketCEA, the HTPB monomer was defined using the empirical formula $C_{10}H_{15.4}O_{0.07}$ (Chmielarek *et al.* 2020).
- Boron-enriched formulation (HTPB/AP/B): to evaluate the energetic enhancement afforded by metallic additives, the second formulation incorporates a 33% mass fraction of amorphous boron according to experimental values (Liu *et al.* 2017). To accommodate this loading while maintaining a constant binder-to-oxidizer ratio, the relative mass fractions were adjusted to 26.8% HTPB and 40.2% AP. The relative mass fractions of HTPB and AP were adopted to preserve the original mass ratio (MR) between internal oxidant and polymeric binder, thereby preventing stoichiometric deviations in the base matrix (as established in the baseline HTPB/AP formulation). This approach ensures that any kinetic variations observed in the vector's trajectory arise exclusively from the thermochemical properties and oxidation efficiency of the boron additive.

Thermochemical model

The thermochemical properties of the combustion products were determined under the assumption of local chemical equilibrium as a function of chamber pressure (P_c) and the air-to-fuel MR. The theoretical vacuum I_{sp} ($I_{sp,vac}$), computed via NASA CEA, was adjusted to yield an effective I_{sp} ($I_{sp,eff}$) that accounts for the non-idealities inherent in a real SFRJ environment. As shown in Eq. 1, the model integrates a composite correction factor:

$$I_{sp,eff} = I_{sp,vac} \cdot \left[1 - x_{boron}\left(1 - \eta_{boron}\right)\right] \cdot \eta_{comb} \tag{1}$$

In this formulation, η_{comb} represents the global combustion efficiency. To enhance predictive accuracy, Eq. 1 incorporates the boron mass fraction (x_{boron}) and the boron-specific combustion efficiency (η_{boron}), the latter being a function of the local thermodynamic state (*Tc(K), Pc(bar)*) according to semi-empirical correlations (Gany 2014; Krishnan and George 1998). These adjustments are critical to mitigate the limitations of the CEA code, which inherently overestimates performance by assuming instantaneous and complete reactions.

The boron combustion efficiency (η_{boron}) is modeled using a hyperbolic tangent formulation in Eq. 2:

$$\eta_{boron} = a + b \tanh \frac{T_c - T_0}{\Delta T} + c \tanh \frac{P_c - P_0}{\Delta P} \quad (2)$$

This mathematical approach was selected to emulate the quasi-sigmoid transition characteristic of boron ignition, triggered by the liquid-to-vapor phase change of the protective B_2O_3 layer. This differentiable framework captures the asymptotic behavior of efficiency in both the inhibited (low-temperature) and saturated (high-temperature) regimes (Natan and Gany 1993). The empirical coefficients (*a, b, c,* T_0, P_0) were calibrated using experimental data to reflect the ignition threshold near 1900 K (King 1972; Yeh and Kuo 1996). Furthermore, the maximum efficiency was constrained to 80% to align with observed losses in SFRJ configurations lacking secondary combustion chambers (Gany 1991).

Intake aerodynamics and stagnation properties

The combustion chamber pressure (P_c) is estimated by evaluating the stagnation pressure recovery across the supersonic inlet. The transition from free-stream to stagnation conditions is governed by Eq. 3, modulated by a recovery factor (η_r) as defined in Eq. 4 (Anderson 2017; Sutton and Biblarz 2017):

$$P_c = P_0 \left(1 + \frac{\gamma - 1}{2} M^2\right)^{\frac{\gamma}{\gamma - 1}} \eta_r \quad (3)$$

$$\eta_r = 1.0 - 0{,}075(M - 1)^{1.35} \quad 1 < \mathrm{M} < 5 \quad (4)$$

Equation 4 follows the MIL-E-5007D standard for fixed-geometry supersonic inlets. The fluid was treated as an ideal gas, with the adiabatic index $\gamma = 1.4$ (ratio of specific heats) adopted to reflect the active degrees of freedom for diatomic molecules (N_2, O_2) at pre-combustion temperatures (Moran and Shapiro 2006).

Atmospheric model and intake flow

To account for the stochastic and altitude-dependent characteristics of the flight environment, the ambient pressure (P_0) and temperature (T_0) were dynamically computed using the U.S. Standard Atmosphere 1976 (1976) model. Equations 5–8 define the conditions adopted in the simulation.

For altitude (h) < 11,000 m:

$$T_0 = 288.15 - 0.0065h \quad (5)$$

$$P_0 = 101325\left({T_0}/{288.15}\right)^{5.2561} \quad (6)$$

For 11,000 m < altitude (h) < 25,000 m:

$$T_0 = 216.65K \quad (7)$$

$$P_0 = 22632e^{-9.81(h-11000)/(287.T_0)} \quad (8)$$

This framework discretizes the atmosphere into geopotential layers, where properties are governed by the hydrostatic equation and the law of perfect gases, assuming a linear lapse rate within the troposphere and lower stratosphere. The accurate determination of P_0 is critical, as it dictates the pressure recovery gradient at the inlet and the pressure-matching conditions at the nozzle exit, directly influencing the net thrust and the I_{sp} throughout the missile's ascent and cruise phases.

The freestream velocity (V_0) and ambient air density (ρ_0) are determined according to the kinematic and atmospheric relations presented in Eqs. 9 and 10 (Anderson 2017; Moran and Shapiro 2006) where the freestream velocity is given in meters per second, the ambient air density is expressed in kilograms per cubic meter and the specific gas constant (R) is defined as 287 $J{\cdot}kg^{-1}{\cdot}K^{-1}$:

$$V_0 = M\sqrt{\gamma R T_0} \tag{9}$$

$$\rho_0 = \frac{P_0}{RT_0} \tag{10}$$

The corresponding air mass flow rate ($\dot{m}_{air}$) ingested by the propulsion system is defined by Eq. 11 (Kubota 2007):

$$\dot{m}_{air} = \rho_0 . V_0 . A_{intake} . \phi_{loss} \tag{11}$$

In this formulation, the density (ρ_0) is derived from the International Standard Atmosphere (ISA) model, establishing a functional dependence where the density decreases monotonically with altitude. This reduction in local density constrains the available oxygen mass for the combustion process, thereby acting as a limiting factor for thrust generation at high altitudes. The term A_{intake} represents the captured streamtube area, while φ_{loss} is a non-dimensional loss coefficient. This factor accounts for aerodynamic inefficiencies and flow spillage associated with oblique and normal shock wave interference at the intake manifold, which deviates a portion of the freestream flow away from the combustor (Sutton and Biblarz 2017).

Thrust and drag model

The propulsive performance is characterized by the net thrust (F_{net}), defined as the difference between the gross thrust generated by the nozzle and the ram drag incurred during air ingestion. Simultaneously, the aerodynamic drag (D) opposes the vehicle's motion, computed as a function of the local air density (ρ_0), freestream velocity (V_0), and the missile's reference cross-sectional area ($A_{missile}$), as shown in Eqs. 12 and 13 (Kubota 2007; Sutton and Biblarz 2017):

$$F_{net} = \left(\dot{m}_{fuel} + \dot{m}_{air}\right) . I_{sp,eff} . g - \left(\dot{m}_{air} V_0\right) \tag{12}$$

$$D = \frac{1}{2}\rho_0 V_0^2 A_{missile} C_d \tag{13}$$

In these expressions, the net thrust (F_{net}) and aerodynamic drag (D) are in Newton (N), and C_d represents the drag coefficient, which accounts for pressure and skin friction effects across the supersonic regime. The drag coefficient was modeled using the linearized theory of supersonic flow, which is designed to capture the transition from transonic drag to the supersonic cruise regime. Eq. 14 describes the variation of drag with Mach number for velocities exceeding Mach 1.2 (Fleeman 2001; Hoerner 1965):

$$C_d = 0.42 + \left({}^{0.12}/_{M}\right) + 0.01M \tag{14}$$

For Mach numbers less than 1.2, a constant drag coefficient of Cd = 0.68 was adopted. This definition of the drag coefficient accurately represents the transonic drag peak, followed by the characteristic decrease observed in the supersonic regime.

Flight dynamics (1-DOF)

The vehicle's translational motion is governed by Newton's second law applied to a variable-mass system. The instantaneous longitudinal acceleration (a) and the mass depletion rate are described by Eqs. 15 and 16:

$$a = \frac{F_{net} - D}{m(t)} \tag{15}$$

$$m(t) = m_{initial} - \int_0^t \dot{m}_{fuel} dt \tag{16}$$

Equation 16 ensures that the total vehicle mass is continuously updated to reflect the consumption of the solid propellant grain during the flight mission.

Numerical method

The governing differential equations are solved over a discretized temporal domain using an explicit first-order Euler scheme (Meghwar *et al.* 2023). At each time step ($\Delta t = 0.5\,s$), the vehicle's state variables – velocity (V) and displacement (S) – are updated based on the acceleration (a_n) and velocity (V_n) computed at the start of the interval, as expressed in Eqs. 17 and 18:

$$V_{n+1} = V_n + a_n \Delta t \tag{17}$$

$$S_{n+1} = S_n + V_n \Delta t \tag{18}$$

Simultaneously, the propellant mass is decremented according to the mass flow rate, ensuring the continuity of mass depletion throughout the simulation. This numerical approach provides a robust and computationally efficient framework for identifying performance trends and evaluating the ballistic envelope of the SFRJ system.

Conceptual model

The numerical simulation framework models a missile launched at an initial velocity of Mach 2.0 at a geopotential altitude of 10 km. The flight profile follows a constant-ascent trajectory with a vertical rate of 100, stabilizing at a cruise altitude of 15 km within the stratosphere. This flight envelope is maintained until the total depletion of the solid propellant. Operating at this altitude minimizes aerodynamic drag due to the lower atmospheric density, thereby optimizing the range and sustaining the high-speed regimes characteristic of SFRJ propulsion.

Model input parameters

The computational model is driven by four primary categories of input data:

- Initial conditions: launch Mach number (M_0) and initial altitude (h_0).
- Propulsion system parameters: fuel mass flow rate ($\dot{m}_{fuel}$), air intake area (A_{intake}), and nozzle expansion ratio (ε). For the comparative analysis of the kinetic and thermochemical properties of the formulations, a constant fuel mass flow rate was assumed, together with a geometrically neutral regression profile for the propellant grain. This methodology enables the isolation of the effects of energy density and net I_{sp} on the vector's trajectory, thereby eliminating combustion transients that could obscure the intrinsic comparative performance of each fuel.
- Vehicle specifications: structural mass, initial propellant mass, and aerodynamic reference area ($A_{missile}$).
- Thermochemical properties: propellant composition (baseline formulation or boron-enriched formulation) and boron mass fraction (x_{boron}).

The reference vehicle is characterized by a cross-sectional area of 0.038 m^2, an air intake area of 0.015 m^2, and a propellant grain mass of 60 kg (assuming a volumetric loading fraction of 80%). The nozzle expansion ratio (ε) is fixed at 5.5.

Performance indicators and outputs

The simulation evaluates the mission effectiveness through the following parameters:

- Propulsive performance: net thrust (F_{net}), net I_{sp} ($I_{sp,liq}$) – accounting for ramjet cycle aerodynamic losses – and effective I_{sp} ($I_{sp,eff}$).
- Flight kinematics: Mach number evolution ($M(t)$), total range, and flight duration (time-to-burn).
- Combustion characteristics: adiabatic flame temperature (T_c) and combustion chamber pressure (P_c).

Vehicle design and operational scenarios

Based on the aforementioned parameters, a hypothetical missile configuration was designed with a diameter of 220 mm, a total length of 2,600 mm, and a structural mass (dry mass) of 150 kg, providing sufficient volume for 60 kg of mass for the propellant grain and additional space for payload (warhead). The propellant grain section is estimated at 1,580 mm in length, with a central port diameter of 110 mm. The conceptual layout is illustrated in Fig. 2.

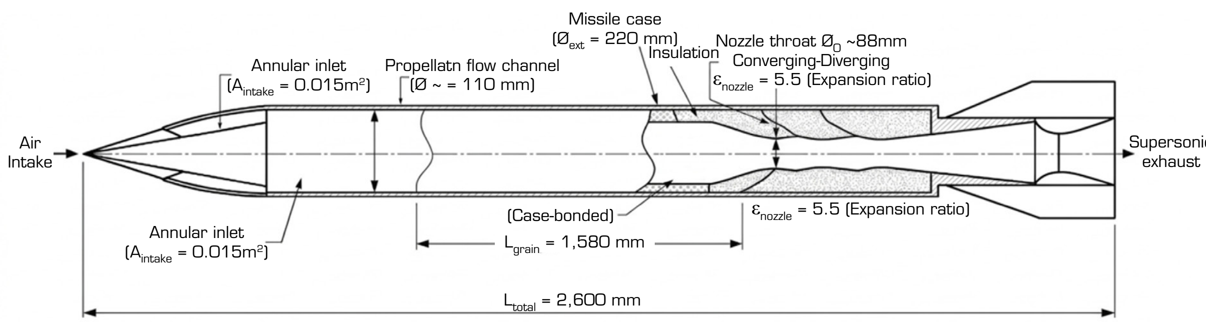

Source: Elaborated by the authors.

Figure 2. Conceptual missile model proposed for simulation.

To assess the influence of boron energetic enhancement on combustion efficiency, two distinct propellant formulations are compared across multiple operational scenarios: baseline formulation (HTPB+AP) and boron-enriched formulation (HTPB+AP+B), evaluated under varying payload capacities (0 kg, 35 kg, and 70 kg).

RESULTS AND DISCUSSION

This section evaluates the numerical simulation results of the SFRJ propulsion model, contrasting the baseline HTPB formulation with the boron-enhanced configuration (33% B by mass). The analysis characterizes the vehicle's kinetic response across various payload capacities, demonstrating how high-energy-density additives modify the mission envelope and enhance tactical viability in long-range stratospheric scenarios.

Internal ballistics and stagnation conditions

The coupling between flight trajectory and internal engine ballistics is illustrated in Fig. 3. Even as the vehicle maintains a constant cruise altitude of 15 km (post 50 s), the combustion chamber stagnation pressure (P_c) exhibits a continuous upward trend. This phenomenon is a direct consequence of the increasing flight Mach number; higher supersonic velocities enhance the isentropic compression efficiency at the air intake, thereby elevating the pressure available for combustion.

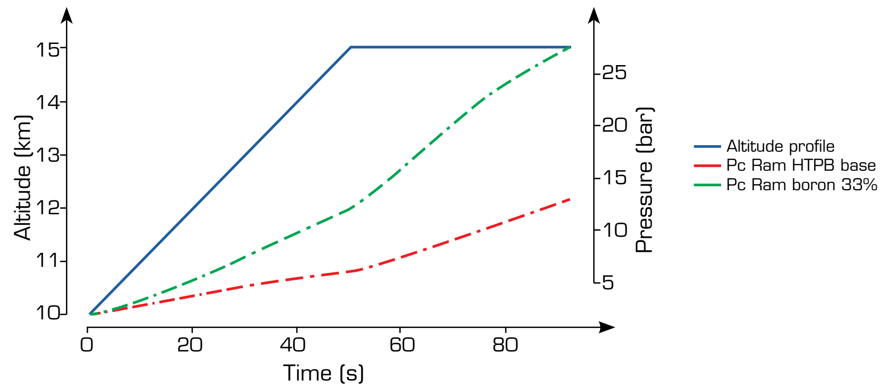

Source: Elaborated by the authors.

Figure 3. Evolution of flight altitude and combustion chamber stagnation pressure (Pc Ram) as a function of time for the 150 kg reference configuration.

The results indicate that optimal thermochemical efficiency is attained during the terminal phase of flight. For boron-enriched propellant formulations, elevated operating pressures are essential, as they promote the mechanical disruption of the passivating boron oxide (B_2O_3) layer. This process markedly decreases the ignition induction period. These observations are consistent with the findings reported by Liu *et al.* (2026), who demonstrated that increased combustion chamber pressure can reduce boron combustion residence time by up to 79% and simultaneously elevate the adiabatic flame temperature by 40% (Liu *et al.* 2026).

Propulsive efficiency and aerodynamic drag

Figure 4 illustrates the progression of net I_{sp} ($I_{sp,net}$) alongside aerodynamic drag for the configurations studied. The boron-enhanced formulation maintains an I_{sp} within the range of 600–700 s, in contrast to the baseline HTPB, which declines to approximately 450 s. These findings are consistent with existing experimental data, which report an I_{sp} of 450 s for conventional SFRJ cycles and theoretical values reaching up to 1,000 s for boron-rich fuels operating at elevated combustion efficiencies (Mandal *et al.* 2023).

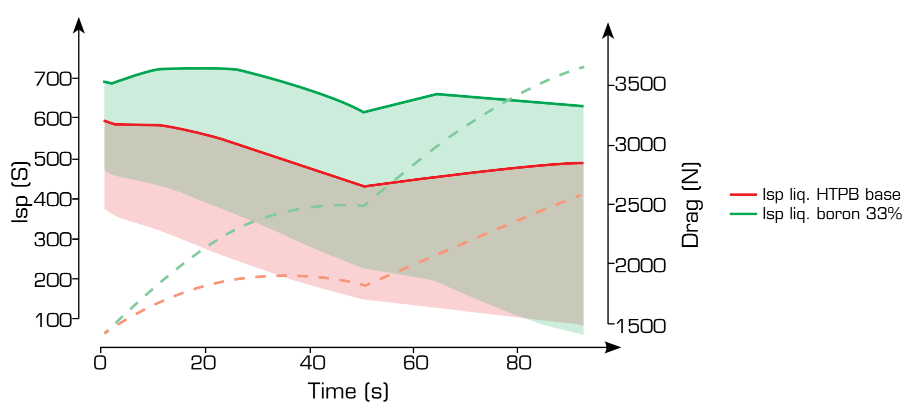

Source: Elaborated by the authors.

Figure 4. Analysis of Net I_{sp} (chemical I_{sp}) and aerodynamic drag losses.

The incorporation of 33% boron yields a mean I_{sp} of 672.9 s, compared to 500.9 s for HTPB, corresponding to a 34.3% enhancement in gravimetric fuel efficiency. The shaded region in Fig. 4 delineates the aerodynamic drag penalty. With increasing Mach number, parasitic drag exhibits exponential growth, reaching a maximum of 3,500 N. Although this aerodynamic resistance contributes to deceleration toward the conclusion of the combustion phase, the higher energy density of boron ensures that gross thrust consistently exceeds the drag penalty, thereby sustaining a superior effective impulse throughout the flight envelope.

Payload sensitivity and kinetic performance

The sensitivity of the vehicle's kinetic performance to varying payloads (0 kg, 35 kg, and 70 kg) is shown in Fig. 5. The energetic superiority of boron is most evident in high-inertia scenarios. In the 0-kg payload configuration, the boron-enhanced missile achieves a terminal velocity of Mach 4.8, compared to Mach 4.1 for the baseline.

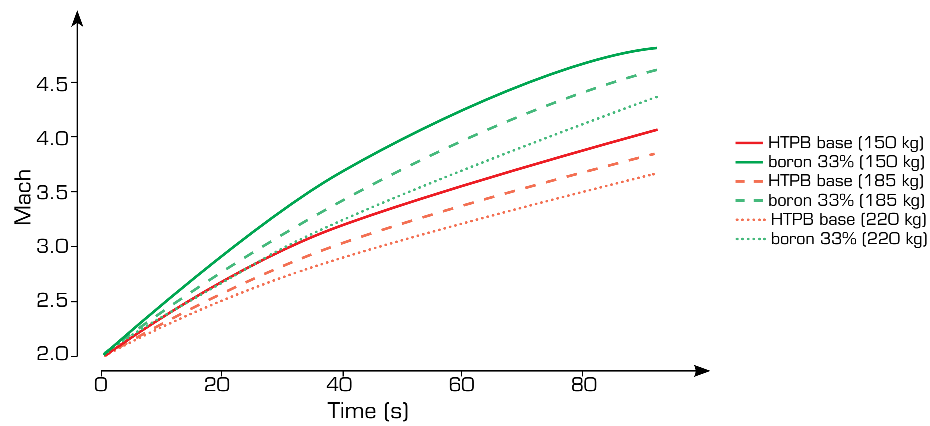

Source: Elaborated by the authors.

Figure 5. Acceleration profile (Mach vs. time) for different payload configurations (0 kg, 35 kg, and 70 kg) – comparison between HTPB base and boron 33%.

Notably, under the maximum payload of 70 kg (total vehicle mass of 220 kg), the boron formulation still exceeds Mach 4.0, whereas the HTPB-only configuration fails to surpass Mach 3.5. This indicates that boron additives are essential for missions requiring heavy warheads without sacrificing terminal kinetic energy.

Operational range and tactical implications

The operational range is significantly extended by the inclusion of boron, as evidenced in Fig. 6. For a fixed burn time of 92 s, the range increases from 88 km (HTPB) to 101.4 km (boron) – a 15.2% gain. This enhancement is not merely a function of thrust but a result of the vehicle's ability to sustain higher cruise velocities, which optimizes the distance traveled per unit of propellant mass – a critical factor in expanding the no-escape zone (NEZ) in air-to-air engagements.

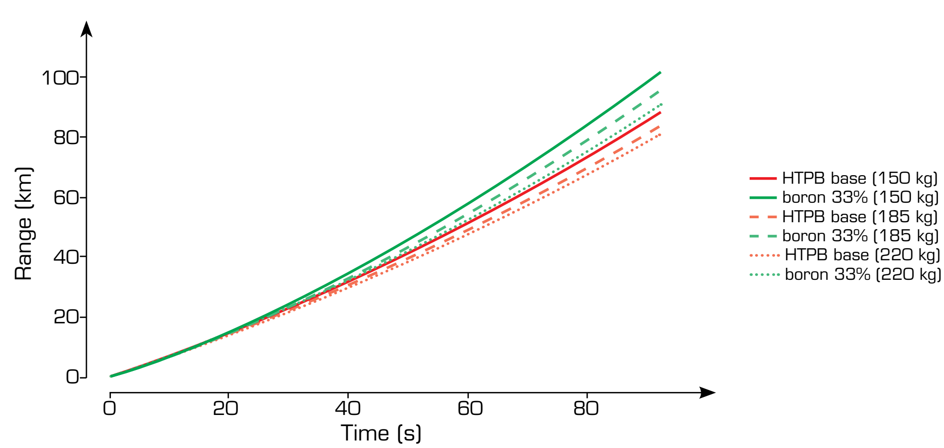

Source: Elaborated by the authors.

Figure 6. Total cumulative range in all payload scenarios.

Furthermore, the 220 kg boron configuration outperforms the lighter 150 kg HTPB baseline in terms of total range (90.4 km vs. 88.0 km). In beyond visual range (BVR) scenarios, the faster time-to-target of the boron-enhanced 150 kg curve translates to reduced intercept times and increased lethality.

Comparative analysis and model validation

While boron offers significant gravimetric heat release advantages, its practical implementation is governed by the complexity of the ignition process. The B_2O_3 coating typically requires temperatures near 1,900 K for removal through evaporation. While the current simulation assumes efficient combustion, future iterations of the code could benefit from coupling chemical kinetics to account for ignition delays caused by oxide layer diffusion barriers (Han *et al.* 2023; Krishnan and George 1998).

The results obtained show a strong correlation with the performance of existing air-launched systems. For instance, comparable missiles operating at 15–20 km altitude report ranges between 80 km and 400 km with cruise speeds near Mach 3 (Fry 2004). Given that our hypothetical model is significantly more compact (2.6 m vs. 3.66 m), the predicted performance levels are realistic and validate the simulation code as a robust preliminary design tool for SFRJ systems.

Conclusions and future work

A comparative analysis between conventional HTPB-based fuel and a boron-doped system reveals that the incorporation of metallic additives is critical for enhancing the performance of SFRJ engines. Computational investigations indicate that the boron-doped formulation achieves a 34.3% increase in average I_{sp} relative to the HTPB baseline, resulting in a value of 672.9 s. This enhancement correspondingly extends the operational range from 88.0 km to 101.4 km, even after accounting for aerodynamic drag losses encountered at elevated velocities.

Furthermore, the boron-based system exhibits notable resilience to increased payload mass. Specifically, the boron-based configuration, when loaded with a maximum payload of 220 kg, surpasses the lighter HTPB configuration (150 kg) in velocity, achieving Mach 4.8 as opposed to Mach 4.1. This capability permits the deployment of heavier warheads without compromising the supersonic performance of the vehicle.

Concomitantly, the observed increases in both maximum Mach number and terminal range substantiate the boron-based formulation as an optimal candidate for BVR missions, substantially enlarging the NEZ of the missile. This finding underscores that the adoption of high-energy-density fuels such as boron constitutes not merely an incremental improvement, but rather a paradigm shift in the lethality and operational envelope of solid ramjet propulsion systems.

Nevertheless, it is essential to acknowledge that, although the present model yields physically consistent trends and numerically stable integration, several simplifying assumptions constrain the quantitative accuracy of the predictions. The utilization of equilibrium chemistry via RocketCEA (derived from NASA CEA) presumes instantaneous reaction kinetics and complete boron oxidation, thus rendering the predicted I_{sp} values as theoretical upper bounds. In practice, realized performance may be diminished due to the influences of particle size and residence time.

The combustion chamber is idealized as a perfectly stirred reactor devoid of axial gradients, omitting considerations for flame stabilization, residence time calculations, and finite-rate chemical kinetics. Chamber pressure is approximated using an ideal total pressure recovery factor, while the drag coefficient is modeled empirically as a Mach-number-dependent scalar, thereby neglecting the effects of Reynolds number, lift-drag interdependence, variations in angle of attack, and the sensitivity of wave drag to geometric factors. The analysis integrates only longitudinal motion, thereby disregarding pitch dynamics, gravitational curvature, thrust-vector-driven ascent, and lateral motion.

Given that the performance of boron-containing propellants in ramjets is determined not solely by their theoretical energy content but also by the system's capacity to realize thermochemical conditions conducive to efficient combustion, future research should refine the model by incorporating a 6-DOF framework coupled with a regression rate dependent on air mass flow. Moreover, experimental validation in supersonic wind tunnels and on static combustion test stands is crucial to reconcile the theoretical efficiency of boron predicted herein with the actual performance losses resulting from two-phase flow phenomena and oxide deposition within the nozzle.

CONFLICTS OF INTEREST

Nothing to declare.

AUTHOR CONTRIBUTIONS

Conceptualization: Monteiro Júnior JFL; **Formal Analysis:** Monteiro Júnior JFL; **Investigation:** Monteiro Júnior JFL; **Methodology:** Monteiro Júnior JFL; **Software:** Monteiro Júnior JFL; **Validation:** Monteiro Júnior JFL; **Visualization:** Monteiro Júnior JFL; **Writing – Original Draft Preparation:** Monteiro Júnior JFL; **Writing – Review & Editing:** Monteiro Júnior JFL and Mendonça F; **Final approval:** Mendonça F.

DATA AVAILABILITY STATEMENT

Simulation parameters and experimental data can be obtained from the corresponding author upon request.

FUNDING

Coordenação de Aperfeiçoamento de Pessoal de Nível Superior
Finance code: 001

DECLARATION OF USE OF ARTIFICIAL INTELLIGENCE TOOLS

In the preparation of this manuscript, the artificial intelligence tool ChatGPT was utilized as an aid for querying search engines for academic work associated with the literature review.

ACKNOWLEDGEMENTS

This study was financed in part by the Coordenação de Aperfeiçoamento de Pessoal de Nível Superior – Brasil (CAPES) Finance Code 001

REFERENCES

Anderson JD Jr (2017) Fundamentals of aerodynamics. 6th ed. New York (NY): McGraw-Hill Education. [accessed Mar 14 2026]. https://www.rexresearch1.com/AeroEngineeringLibrary/FundamentalsAerodynamics.pdf

Ao W, Yang W, Wang Y, Zhou J, Liu J, Cen K (2014) Ignition and combustion of boron particles at one to ten standard atmosphere. J Propuls Power 30(3):760-764. https://doi.org/10.2514/1.B35054

Chmielarek M, Maksimowski P, Cieślak K, Gołofit T, Drozd H (2020) Study of the synthesis of GAP-HTPB-GAP liquid copolymer. Cent Eur J Energ Mater 17(4):566-583. https://scispace.com/pdf/study-of-the-synthesis-of-gap-htpb-gap-liquid-copolymer-1x5dppe9yq.pdf

Fleeman EL (2001) Tactical missile design. Reston (VA): American Institute of Aeronautics and Astronautics. [accessed Mar 14 2026]. https://ftp.idu.ac.id/wp-content/uploads/ebook/tdg/MILITARY%20PLATFORM%20DESIGN/Tactical%20Missile%20Design.pdf

Fry RS (2004) A century of ramjet propulsion technology evolution. J Propuls Power 20(1):27-58. https://doi.org/10.2514/1.9178

Gany A (1991) Combustion of boron-containing fuels in solid fuel ramjets. Int J Energetic Mater Chem Propuls 2(1-6): 91-112. https://doi.org/10.1615/IntJEnergeticMaterialsChemProp.v2.i1-6.40

Gany A (2014) Thermodynamic limitation on boron energy realization in ramjet propulsion. Acta Astronaut 98:128-132. https://doi.org/10.1016/j.actaastro.2014.01.023

Gordon S, McBride B, Zeleznik FJ (1984) Computer program for calculation of complex chemical equilibrium compositions and applications. Supplement 1: Transport properties. Cleveland (OH): National Aeronautics and Space Administration, Lewis Research Center. NASA-TM-86885. [accessed Mar 14 2026]. https://ntrs.nasa.gov/citations/19850008354

Han L, Wang R, Chen W, Wang Z, Zhu X, Huang T (2023) Preparation and combustion mechanism of boron-based high-energy fuels. Catalysts 13(2):378. https://doi.org/10.3390/catal13020378

Hoerner SF (1965) Fluid-dynamic drag: theoretical, experimental and statistical information. 2nd ed. Midland Park (NJ): Hoerner Fluid Dynamics. [accessed Mar 14 2026]. http://ftp.demec.ufpr.br/disciplinas/TM240/Marchi/Bibliografia/Hoerner.pdf

King MK (1972) Boron ignition and combustion in air-augmented rocket afterburners. Combust Sci Technol 5(1):155-164. https://doi.org/10.1080/00102207208952516

Krishnan S, George P (1998) Solid fuel ramjet combustor design. Prog Aerosp Sci 34(3-4):219-256. https://doi.org/10.1016/S0376-0421(98)00005-0

Kubota N (2007) Propellants and explosives: thermochemical aspects of combustion. 2nd completely revised and extended ed. Weinheim (Germany): Wiley-VCH. https://doi.org/10.1002/9783527610105

Liang D, Liu J, Xiao J, Xi J, Wang Y, Zhang Y, Zhou J (2015) Energy release properties of amorphous boron and boron-based propellant primary combustion products. Acta Astronaut 112:182-191. https://doi.org/10.1016/j.actaastro.2015.03.019

Liang D, Liu J, Zhou Y, Zhou J, Cen K (2017) Ignition and combustion characteristics of molded amorphous boron under different oxygen pressures. Acta Astronaut 138:118-128. https://doi.org/10.1016/j.actaastro.2017.05.019

Liu J, Liang D, Xiao J, Chen B, Zhang Y, Zhou J, Cen K (2017) Composition and characteristics of primary combustion products of boron-based propellants. Combust Explos Shock Waves 53(1):55-64. https://doi.org/10.1134/S0010508217010099

Liu Y, Li S, Chen S, Yao H, Huang X, Li Z, Xu X, Song J (2026) High pressure effect on combustion characteristics and reaction mechanism of single boron carbide microparticles. Combust Flame 284:114689. https://doi.org/10.1016/j.combustflame.2025.114689

Mandal S, Hashim SA, Roy A, Karmakar S (2023) A short review of challenges and prospects of boron-laden solid fuels for ramjet applications. FirePhysChem 3(3):179-200. https://doi.org/10.1016/j.fpc.2023.06.001

Meghwar T, Kumar P, Khokhar RB, Shaikh AA, Hincal E, Anwar Solangi M (2023) Development of an explicit iterative numerical scheme over the modified Euler's method. VFAST Trans Math 11(1):107-120. https://doi.org/10.21015/vtm.v11i1.1419

Moran MJ, Shapiro HN (2006) Fundamentals of engineering thermodynamics. 5th ed. Hoboken (NJ): John Wiley & Sons. [accessed Mar 14 2026]. https://www.arma.org.au/wp-content/uploads/2017/03/Fundamentals-of-Engineering-Thermodynamics-by-Michael-J.Moran-Howard-N.-Shapiro.pdf

Natan B, Gany A (1993) Combustion characteristics of a boron-fueled solid fuel ramjet with aft-burner. J Propuls Power 9(5):694-701. https://doi.org/10.2514/3.23677

Ou M, Yan L, Tang J, Huang W, Chen X (2017) Thermodynamic performance analysis of ramjet engine at wide working conditions. Acta Astronaut 132:1-12. https://doi.org/10.1016/j.actaastro.2016.11.036

Pang W, De Luca LT, Fan X, Glotov OG, Zhao F (2019) Boron-based fuel-rich propellant: Properties, combustion, and technology aspects. 2nd ed. Boca Raton (FL): CRC Press. https://doi.org/10.1201/9780429030680

Sandall ET, Kalman J, Quigley JN, Munro S, Hedman TD (2017) A study of solid ramjet fuel containing boron-magnesium mixtures. Propuls Power Res 6(4):243-252. https://doi.org/10.1016/j.jppr.2017.11.004

Sutton GP, Biblarz O (2017) Rocket propulsion elements. 9th ed. Hoboken, NJ: John Wiley & Sons. [accessed Mar 14 2026]. https://ftp.idu.ac.id/wp-content/uploads/ebook/tdg/DESIGN%20SISTEM%20DAYA%20GERAK/Rocket%20Propulsion%20Elements.pdf

U.S. Standard Atmosphere 1976 (1976) Washington, DC: National Oceanic and Atmospheric Administration; National Aeronautics and Space Administration; United States Air Force; 1976. Report No.: NASA-TM-X-74335, NOAA-S/T-76-1562. [accessed Mar 14 2026]. https://ntrs.nasa.gov/citations/19770009539

Yang D, Liu R, Li W, Yan QL (2023) Recent advances on the preparation and combustion performances of boron-based alloy fuels. Fuel 342:127855. https://doi.org/10.1016/j.fuel.2023.127855

Yeh CL, Kuo KK (1996) Ignition and combustion of boron particles. Prog Energy Combust Sci 22(6):511-541. https://doi.org/10.1016/S0360-1285(96)00012-3